2008

A Novel Wide-Angle Laser Triangulation Method For Obstacle Detection

Kaveh Sahba
Edith Cowan University

Kamal Alameh
Edith Cowan University

Clifton Smith
Edith Cowan University

A novel wide angle laser triangulation method for obstacle detection

Kaveh Sahba[a], Kamal E. Alameh [a],Clifton L. Smith[b]
[a]Western Australia Centre of Excellence for MicroPhotonic Systems; [b]School of Engineering,
Edith Cowan University, 100 Joondalup Dve, Joondalup, 6027 Western Australia.

ABSTRACT

Indoor active triangulation to laser spots generated by quasi-cylindrical cavity is demonstrated. Principal ray trajectory is modeled using a system of linear equations and fundamental ray geometry. Each ray's unique outgoing angle and baseline is calculated and used to derive the range to the corresponding spot. Above 98% accuracy is achieved over an approximate range of 5m, demonstrating a novel motionless laser scanning technique with a wide scanned angle and no moving parts.

Keywords: Laser sensors, laser range finder, optical design

1. INTRODUCTION

Currently, laser beam deflection is achieved by electro-mechanically driving single or multi-faceted rotating polygon mirrors, usually in combination with galvanometric/resonant mirrors. Mechanical laser scanners have several drawbacks, namely, (i) the intrinsic motion of the mirrors and motors cause scanning problems which are the hardest to quantify and correct, (ii) the acceleration time taken to reach the constant scanning speed from a stationary position can result in range measurements being stored at the wrong corresponding points in the scanned image, (iii) the performance in terms of maintaining an accurate deflection beam path is prone to manufacturing tolerances, and (iv) dynamic track and jitter errors are caused by tolerances for polygon machining errors, mounting errors, mounting-hub errors, random wobble caused by ball bearings, motor cogging and torque variations [1]. Laser scanning, in general, is much more sensitive to vibration than a multi-beam stationary optic approach [2]. In particular, mirror device scanners are slow, bulky and expensive [3] and being inherently mechanical they wear out as a result of acceleration, cause deflection errors and require regular calibration [4]. A comprehensive discussion of rotary and galvanometer/resonant mirror scanning errors can be found in [5].

In this paper, an approach to generating multiple beams over a wide angle with no moving parts and deriving the range to the corresponding laser spots falling on the surrounding perimeter is demonstrated. A novel optical piece in the form a cylindrical quasi-cavity with 45° curvature has been fabricated and used to perform structured laser light projection in the form of a spot array. By applying nano-layered thin film coatings on both interfaces, at every reflection with the outer interface, a fraction of the light is transmitted through the cavity, generating a laser spot. The reflected power undergoes further reflections within the cavity to generate many subsequent laser spots.

The active laser triangulation arrangement is modelled using a system of linear equations where principal rays and components are plotted as straight lines and circles. Using this model and ray geometry, each outgoing beam's angle, bearing and baseline distance are calculated. Ranging is conducted in a controlled indoors environment and yields high accuracy (>98%) with small standard deviation, validating the algebraic approach to simulating the arrangement.

2. QUASI-CYLINDRICAL OPTICAL CAVITY MULTI-LASER BEAM GENERATION

The custom concentric concave-convex cavity, shown in Fig. 1, comprises an inner interface and outer interface of radii R_1 and R_2, respectively, separated by a BK-7 glass medium of thickness $d = R_2-R_1$, and entrance and exit windows. Light transmission is achieved by depositing nano-layered thin film coatings on both interfaces. The rear side is deposited with a highly reflective coating (R≥99%) and the front side with a partial transmission coating (T≤13%), effective over the 600 – 900nm waveband. At every reflection with the outer interface, a fraction of the light is transmitted through the cavity thus generating a laser spot. The reflected power undergoes further reflections within the cavity to generate subsequent laser spots. The inter-beam spacing is controlled by adjusting the incident angle of the injected laser beam.

19th International Conference on Optical Fibre Sensors, edited by David Sampson, Stephen Collins, Kyunghwan Oh,
Ryozo Yamauchi, Proc. of SPIE Vol. 7004, 70046E, (2008) 0277-786X/08/$18 doi: 10.1117/12.786532

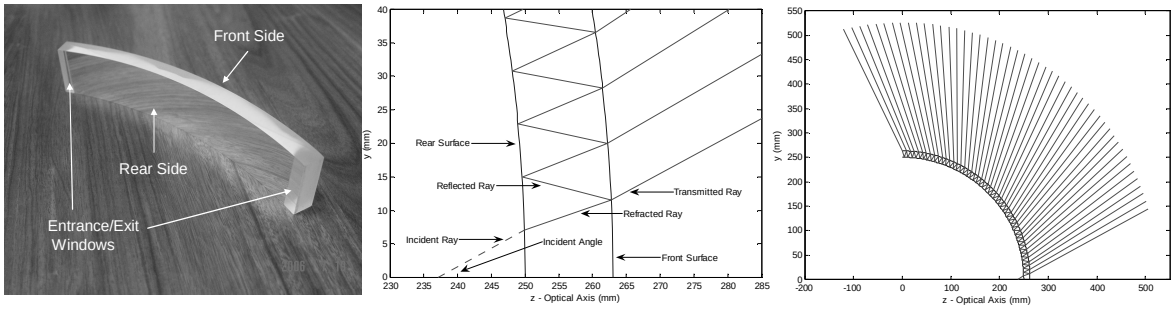

(a) (b) (c)

Fig. 1. (a) Quasi-cylindrical cavity, (b) entrance close-up plot and (c) ray trajectory plot over 90º.

3. ACTIVE TRIANGULATION GEOMETRY FUNDAMENTALS

The basic geometry of an active triangulation system involves an imaging device of focal length f positioned in line with the Z-axis, with the X-axis running through its lens centre. To the left of the lens, at a baseline distance β, a laser source launches a light beam at a variable angle w. The image point lying on the u plane, together with β, w and f determine the X and Z coordinates of the illuminated target point. The forward distance, z and horizontal distance, x to the projected laser spot from the lens centre are given by [6]:

$$x = f \cdot \frac{\beta}{f\cot(w) - u} \cdot u\,, \tag{1}$$

$$z = f \cdot \frac{\beta}{f\cot(w) - u} \cdot f\,. \tag{2}$$

The direct distance from the lens centre to the projected spot is $R = \sqrt{x^2 + z^2}$.

4. LASER TRIANGULATION SETUP INCLUDING THE OPTICAL CAVITY

Fig. 2(a) illustrates principal rays of the novel triangulation system incorporating the quasi-cylindrical optical cavity. Adopting the linear algebraic ray tracing method from [7], cavity interfaces and rays are predicted using equations for circles and straight lines, respectively. Fig. 2 indicates that each outgoing laser beam has unique β and w values with respect to the rotated lens line, L. Fig. 2(b) shows the experimental setup that was used to demonstrate active triangulation using the quasi-cylindrical optical cavity of 45° curvature.

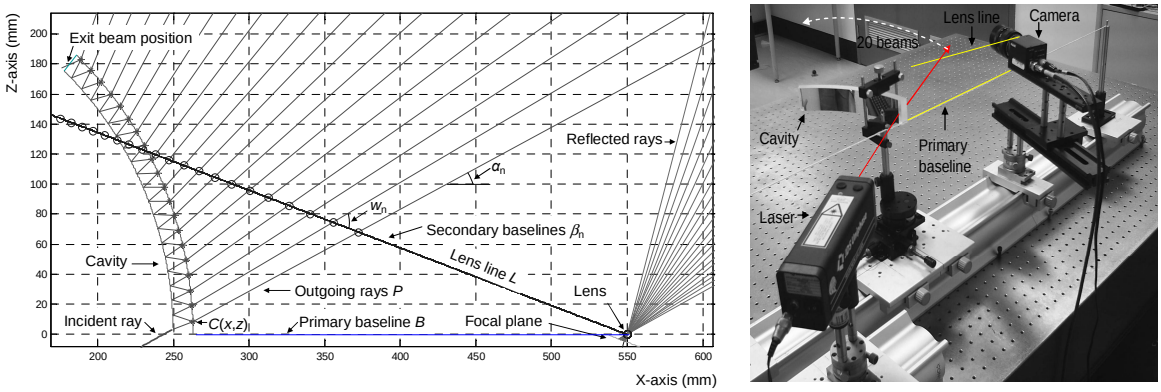

(a) (b)

Fig. 2. (a) Principal ray plot and (b) photo of the experimental setup using the quasi-cylindrical optical cavity.

Each ray's outgoing angle with respect to the lens line of slope L_m is:

$$w = \tan^{-1}\left(\frac{\alpha - L_m}{1 + \alpha \cdot L_m}\right). \tag{3}$$

The baseline distance, β is calculated as:

$$\beta = \sqrt{(\beta(x) - L(x)) + (\beta(z) - L(z))}. \tag{4}$$

Twenty laser spots were generated when an incident laser beam was injected through the entrance window. The cavity's orientation and position were adjusted using a tilt and precision translation stage, respectively. Note that the number of outgoing beams depends on the position and incident angle of the input laser beam.

The incident beam was produced by a 632.3nm, 1mW, HeNe laser, which was mounted onto a rotating stage with a 0.5° step. To image the projected laser spots, a ½" interline transfer CCD imager was employed, comprising of 768(H) × 494(V) pixels of size 8.4 × 9.8μm. A C-mount TV lens of focal length f = 12.5mm, focused at infinity, collected the reflected laser light. The lens iris was adjusted appropriately to avoid saturation of the imaged spot. Images from the camera were digitized in 12-bit form using a Spiricon Plug and Play PCI frame grabber. Both the quasi-cavity and camera were staged on a common rail. The distance between them defines the primary baseline, B = 0.3m, as shown in Fig. 2(b). One image was acquired of spots 11 to 20 to validate the concept. The camera angle, L_θ, was set at 73º with respect to the X-axis. Three screens were placed between the camera and the laboratory wall to demonstrate that a closer object's range, with respect to the wall could be accurately determined.

An intensity profile was taken across every spot and the digital pixel array processed to find the peak intensity pixel position using the Gaussian sub-pixel peak position estimator algorithm defined in [8] as follows:

$$\delta = \frac{1}{2}\frac{\ln(f(u-1)) - \ln(f(u+1))}{\ln(f(u-1)) - 2\cdot\ln(f(u)) + \ln(f(u+1))}, \tag{5}$$

where u is the pixel position of the observed peak sensor reading with an intensity of $f(u)$. The peak position of a laser beam spot imaged at pixel position u is offset by the estimated pixel fraction δ.

To calibrate the system, constrained nonlinear optimization was used to find the optimal values of parameters subject to uncertainties. The optimization was based on the minimization of the least square error, namely:

$$\sum_{i=11}^{20}\left(R_i - \hat{R}_i\right), \tag{6}$$

where R_i is the actual range and $\hat{R}_i$ is the calculated range for the i^{th} laser spot. The two most significant uncertainties in the experimental setup were:

1. The imager pixel size. Although already manufacturer-specified, the pixel pitch was not known, thus producing error in calculating the captured ray's physical position on the image sensor. Hence, a pixel scaling factor, η, was used. In this experiment, η = 1.0137.
2. The angle of the lens line, L_θ, which was not accurate since the camera's rotating stage was fixed using a single bolt. The optimized L_θ was 72.237º.

Other uncertainties included the exact position of the lens centre along the optical axis within the complex TV lens system and the centre-to-centre alignment of the image sensor and lens. An alignment error attributed to the primary baseline, B, running directly through the lens centre can exist. Note that if the camera was displaced vertically, the lens would not be in the same plane as B, and this would lead to inaccuracy in range measurements.

5. RESULTS AND DISCUSSION

Four frames of the imaged beam spots were taken and the mean range, R, for every spot was obtained as shown in Fig. 3 (a). Since the standard deviations of the mean range were small, they were plotted separately as shown in Fig. 3(b).

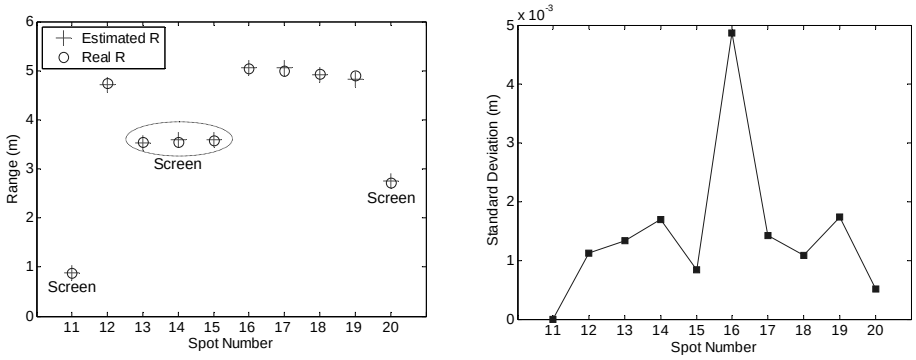

(a) (b)

Fig. 3. (a) Range measurement results for spots 11 to 20 falling on the laboratory perimeter and (b) standard deviation of the mean ranges.

Note that Fig. 3(a) shows very good agreement between the measured and calculated ranges, validating the method of deriving β and w using linear algebra as described in Section 4. Note also that the maximum standard deviation of the mean range is under 0.005m, demonstrating the stability of the system. The minimum ranging accuracy achieved is 98.59%, for spot 17.

6. CONCLUSION

Accurate triangulation-based ranging to multiple laser spots generated over a wide angle by a novel waveguide component has been demonstrated. A system of linear equations has been used to simulate the principal rays and components of the triangulation system and obtain the unique baseline distance and outgoing angle of every beam.

Range accuracy has been discussed, showing strong dependence on the precise instrumentation of the system arrangement. Calibration has been achieved by non-linearly optimizing values for uncertain instrumental parameters within realistic constraints, and more than 98% accuracy has been observed over a range of 5m, validating the concept of a novel motionless wide angle laser scanning technique. With the absence of moving parts, this type of scanning is particularly useful where robustness and mean time between failures is critical, such as perimeter security, collision avoidance and navigation.

REFERENCES

[1] Stutz, G. (2005). Guiding Light, in *SPIE's oemagazine*, *5*, 25-27.

[2] C. Taylor, D. Barlett, E. Chason and J. Floro, "A Laser-Based Thin-Film Growth Monitor," The Industrial Physicist, **4**, 26-30 (1998).

[3] O. Elkhalili, M. O. Schrey, P. Mengel, M. Petermann, W. Brockherd and B.J. Hosticka, "A 4 X 64 pixel CMOS image sensor for 3-D measurement applications," IEEE Journal of Solid State Circuits, **39**, 1208-1212 (2004).

[4] K. Schnadt and R. Katzenbeißer. (2004). "Unique Airborne Fiber Scanner Technique for Application-Oriented LIDAR Products," Proceedings of the ISPRS Working Group VIII/2, 36.

[5] L. F. Marshall, Handbook of Optical and Laser Scanning (Marcel Dekker Inc., 2004).

[6] P. J. Besl, "Active, Optical Range Imaging Sensors," Machine Vision and Applications, **1**, 127-152 (1988).

[7] K. Sahba, K. E. Alameh, C. L. Smith and A. Paap, "Cylindrical quasi-cavity waveguide for static wide angle pattern projection," Optics Express, **15**, 3023-3030 (2007).

[8] R. B. Fisher and D.K. Naidu, "A Comparison of Algorithms for Subpixel Peak Detection," in Sanz (ed.) Advances in Image Processing, Multimedia and Machine Vision (Springer-Verlag, 1996).